ORIGINAL SCIENTIFIC PAPER

CROATICA CHEMICA ACTA

Croat. Chem. Acta **2025**, *98*(3)
Published online: August 31, 2025
DOI: 10.5562/cca4170

HKD 1926

Molecular Weight Dependent Adsorption of Polyacrylic Acid on Porous and Nonporous Alumina Influenced by pH and Surface Accessibility

Nikolina Filipović,[1] Berislav Marković,[2,*] Dalibor Tatar,[1] Ponisseril Somasundaran[3]

[1] University of Osijek, Department of Chemistry, Cara Hadrijana 8/A, 31000 Osijek, Croatia
[2] University of Osijek, Faculty of Dental Medicine and Health, Crkvena 21, 31000 Osijek, Croatia
[3] Columbia University, 905 SW Mudd, 500 W 120th Street, New York, NY 10027, USA
* Corresponding author's e-mail address: bmarkovic@fdmz.hr

RECEIVED: March 17, 2025 * REVISED: August 06, 2025 * ACCEPTED: August 07, 2025

Abstract: The adsorption of polymers at solid–liquid interfaces is fundamental to processes such as flocculation, dispersion, and surface modification. While polymer adsorption density typically increases with molecular weight, this study demonstrates that substrate porosity can invert this trend. The adsorption behavior of polyacrylic acid (PAA) with molecular weights of 5000, 150000 and 800000 g mol^{-1} was investigated on two types of alumina powders: porous Linde A and non-porous AKP-50. Comprehensive characterization using X-ray diffraction (XRD), Scanning Electron Microscopy (SEM), zeta potential measurements, particle size analysis, Brunnauer–Emmett–Teller (BET) nitrogen adsorption, and mercury intrusion porosimetry confirmed the highly porous structure of Linde A and the compact, non-porous nature of Sumjitomo AKP-50. Adsorption experiments performed at pH 4, 7, and 10 revealed a complex interplay between polymer molecular weight, substrate porosity and pH. On non-porous AKP-50, adsorption density increased with molecular weight, consistent with established theory. In contrast, on porous Linde A, the lowest molecular weight PAA exhibited the highest adsorption density, attributed to greater accessibility within narrow pores. This reverse trend was most pronounced at low pH (4), where the polymer chains are coiled. At high pH, where the chains are elongated due to ionization, adsorption density became almost independent of molecular weight, as larger molecules could also enter the pore structure. A correlation between polymer molecular size and alumina pore size distribution was established, and a model of selective pore accessibility is proposed. These findings challenge conventional understanding and highlight the critical influence of substrate morphology and environmental conditions on polymer adsorption, providing valuable insights for the design of tailored polymer-based surface treatments and dispersants.

Keywords: alumina, adsorption density, molecular weight, polyacrylic acid, porosity.

INTRODUCTION

POLYMERS are widely employed in a variety of industrial applications such as flocculation, stabilization, dispersion, and surface modification, where their interfacial behavior plays a critical role in determining overall system performance. One of the most influential parameters affecting polymer adsorption density at solid–liquid interfaces is the polymer's molecular weight. In general, polymers with higher molecular weights tend to exhibit stronger adsorption density compared to their lower molecular weight counterparts, owing to their extended chain length, greater number of functional groups, and a higher density of potential interaction sites with the substrate surface.[1–8] This well-established trend, however, has been predominantly confirmed under idealized laboratory conditions using smooth, non-porous model substrates. In real-world systems, solid surfaces rarely exhibit such simplicity; instead, they are often characterized by varying degrees of roughness, chemical heterogeneity, and porosity, all of which can significantly impact the nature and extent of polymer adsorption. Among these surface characteristics, porosity stands out as a particularly critical but comparatively underexplored factor.[9–13] Porous substrates introduce a spatially constrained environment, which inherently limits the access of polymer chains based on their molecular size and

conformation. Larger polymers may experience steric exclusion or limited diffusion into narrower pores, while smaller chains might access a broader range of surface area within the porous network.[14,15] This suggests that adsorption density behavior may deviate significantly from classical trends when porosity is present, and that molecular weight may not always correlate positively with the extent of adsorption. While earlier studies on polymer adsorption have mostly employed monodisperse polymers interacting with idealized flat, smooth, and non-porous surfaces,[16–18] real polymers are often polydisperse,[19–22] and industrially relevant solid substrates typically feature heterogeneous, irregular, and porous surfaces.[23–25] These deviations from ideality introduce additional complexities into the adsorption process, such as steric hindrance at pore entrances, restricted diffusion into the pore network, and variable chain conformations depending on environmental factors like pH. Moreover, polymer adsorption density is fundamentally different from that of small molecules such as ions or surfactants due to the conformational flexibility of polymer chains and the multiplicity of their interaction sites.[3–8,26]. This complexity makes it challenging to develop universal models that can accurately describe polymer adsorption density under realistic conditions. Although theoretical and computational approaches have offered insights into adsorption phenomena,[13–15,27,28] their practical application is often constrained by the need to simplify complex systems and by the limited availability of precise experimental data.

In this study, we systematically investigate the influence of substrate porosity on the adsorption density behavior of polyacrylic acid (PAA) with three distinct molecular weights (5000, 150000 and 800000 g mol^{-1}). Two types of alumina were selected to represent contrasting surface morphologies: porous Linde A and non-porous AKP-50. Adsorption experiments were conducted at three pH values (4, 7, and 10) to explore how polymer conformation, modulated by degree of ionization, influences adsorption dynamics across different surface types. Comprehensive surface characterization including scanning electron microscopy (SEM), BET nitrogen adsorption, mercury intrusion porosimetry, and zeta potential measurements was used to elucidate the relationship between polymer size, conformation, and pore accessibility. Our findings reveal a reversal of the commonly expected molecular weight–adsorption trend on porous substrates, which we attribute to a size-exclusion mechanism favoring smaller polymer chains. We propose a conceptual model to describe this phenomenon, incorporating polymer conformation and pore structure as key variables. This work contributes to a deeper understanding of polymer adsorption under realistic surface conditions and provides valuable insights for the rational design of polymer-based surface modifiers, dispersants, and treatment agents for use in porous materials.

EXPERIMENTAL

Chemical and Reagents

Polyacrylic acid (PAA) samples used in this study were purchased from Polysciences Inc. The low molecular weight PAA (M_w = 5000 g mol^{-1}) was supplied as a concentrated aqueous solution at 50 wt. %, while the intermediate molecular weight PAA (M_w = 150000 g mol^{-1}) was supplied at 25 wt. %. A second batch of the low molecular weight PAA (M_w = 5000 g mol^{-1}) was also received at 25 wt. % for comparative purposes. The high molecular weight PAA (M_w = 800000 g mol^{-1}) was provided in powder form. According to the manufacturer, all polymer samples exhibit relatively high polydispersity (M_w/M_n = 3–4) and contain trace levels of residual isopropanol (0.5 %), acrylic acid (0.1 %), and propionic acid (0.1 %). Two types of alumina powders were selected as substrates for adsorption studies: Linde Alumina Polishing Powder Type A, manufactured by Union Carbide Corp. (USA), and AKP-50 Alumina, produced by Sumitomo Chemical Co., Ltd. (Japan). Linde A alumina is synthesized by controlled calcination of ammonium aluminum sulfate (alum) and is primarily used as a polishing material. Manufacturer-provided properties of this powder are listed in Table 1. AKP-50 is a high-purity α-alumina powder obtained via hydrolysis of aluminum alkoxide. This synthesis method yields fine, uniform α-alumina crystals with narrow particle size distribution and excellent purity. Technical specifications supplied by the manufacturer for AKP-50 are summarized in Table 2.

Triply distilled water was used throughout this study (specific conductivity: 1.2–1.5 × 10^{-6} S cm^{-1}). Fisher-certified hydrochloric acid and sodium hydroxide solutions were used for pH adjustment. All inorganic reagents were of analytical grade and were purchased from Fisher Scientific (USA). Unless otherwise stated, the ionic strength was maintained at 0.03 mol dm^{-3} using NaCl.

Table 1. Manufacturers data on Linde Alumina Polishing Powder Type A.

Crystal form	Purity, Al_2O_3 %	Particle size, μm	Packed density, g cm^{-3}	B.E.T. surface area, m^2 g^{-1}
90 % α–Al_2O_3 10 % γ–Al_2O_3	99.98	0.3 (crystal)	0.30	10 – 18
Impurities, ppm				
Na	Si	Ca	Ga	Zn
≤ 60	≤ 100	≤ 50	≤ 30	≤ 19

Table 2. Manufacturers data on AKP-50 alumina.

Crystal form	Purity, Al_2O_3 %	Particle size, μm	Packed density, g cm^{-3}	B.E.T. surface area, m^2 g^{-1}
α–Al_2O_3	< 99.99	0.1 – 0.3	0.9 – 1.3	9 – 15
Impurities, ppm				
Si	Na	Mg	Cu	Fe
≤ 25	≤ 10	≤ 10	≤ 10	≤ 20

Methods – Substrate Characterization

MINERALOGICAL ANALYSIS BY X-RAY DIFFRACTION

Qualitative phase analysis of the two alumina samples (AKP-50 and Linde A) was carried out using powder X-ray diffraction (PXRD). Diffraction data were collected on a Philips 300 diffractometer operating at 35 kV and 25 mA, using CuKα radiation (λ = 1.54 Å) and equipped with a graphite monochromator. The obtained diffraction patterns were used to identify the crystalline phases present in each sample.

PARTICLE SIZE DISTRIBUTION

The particle size of AKP-50 and Linde A alumina powders spans a wide range from submicron dimensions up to several tens of micrometers. To accurately determine the particle size distribution across this range, three complementary techniques were applied: multi-angle light scattering, forward light scattering, and image analysis. For the AKP-50 sample, measurements were performed using a Brookhaven Multi-Angle Light Scattering System based on photon correlation spectroscopy. The system comprised a Brookhaven BI-8000AT Digital Correlator, a BI-200SM Goniometer, and a Lexel Model 95 Ion Laser. The alumina was suspended in triply distilled water at a concentration of 0.01 wt. % and homogenized via ultrasonication. Measurements were carried out at a fixed scattering angle of 90°, using a laser wavelength of 488 nm and a power output of 100 mW. To broaden the particle size detection range, forward light scattering measurements were performed using a Microtrac Model 7995-11 Particle Size Analyzer (Leeds & Northrup Instruments, USA). This instrument detects scattered light from flowing particle suspensions across 15 photodetector channels, enabling determination of particle sizes from 0.9 μm to 125 μm. Due to its morphology, the Linde A sample was not suitable for light scattering analysis. Instead, particle size distribution was determined by image analysis using an Omicon 3000 Image Analysis System (Bausch & Lomb, USA), calibrated with a reference slide containing 100 μm circular patterns. Approximately 10,000 particles were analyzed, and the longest dimension of each particle was used as the size metric.

ZETA POTENTIAL

The zeta potential of the alumina particles was measured by microelectrophoresis using a Pen Kem Lazer Zee Meter Model 501. The instrument features a rectangular fused silica electrophoresis cell, with the stationary fluid layer located approximately 230 μm from the top or bottom of the chamber. Particle movement was observed under a microscope. A custom optical prism system, connected to a galvanometer, enabled real-time visual tracking and scanning of particle motion. The zeta potential was recorded at the point where particles appeared stationary in the visual field, providing a reliable measure of surface charge under experimental conditions.

SPECIFIC SURFACE AREA BY NITROGEN ADSORPTION (BET METHOD)

The specific surface area of the alumina powders was determined using the multipoint Brunauer–Emmett–Teller (BET) method. Nitrogen adsorption measurements were performed at 77 K using a Quantasorb Sorption System (Quantachrome Corporation, USA). A five-point BET plot was constructed using relative pressure values ranging from 0.05 to 0.35. Care was taken to maintain stable experimental conditions and ensure accurate adsorption data. These measurements provided insight into surface characteristics relevant to porosity and accessible surface area.

MERCURY INTRUSION POROSIMETRY FOR PORE STRUCTURE CHARACTERIZATION

Mercury intrusion porosimetry was performed using the AutoPore II 9220 Automated Mercury Porosimeter (Micromeritics Instrument Corporation, USA), which enables pore size distribution measurements in the range of 0.003 to 360 μm under pressures up to 414 MPa. The method is based on the principle that the applied pressure is inversely proportional to the diameter of the penetrated pores. This technique allows for accurate characterization of macropores and mesopores with high precision.

ADSORPTION PROCEDURE

Adsorption experiments were carried out by adding polymer solutions of various concentrations to pre-equilibrated alumina slurries, under strictly controlled pH and ionic strength conditions. Polyacrylic acid (PAA) solutions were prepared either by dilution of commercial aqueous stock solutions or by dissolution of powdered PAA followed by serial dilution. Sodium chloride (0.03 mol dm^{-3}) was used as the background electrolyte in all experiments to maintain constant ionic strength. All experiments were performed at room temperature (22–23 °C), and pH was adjusted using dilute hydrochloric acid or sodium hydroxide solutions. In a typical adsorption procedure, 0.5 g of alumina powder was mixed with 4.5 g of 0.03 mol dm^{-3} NaCl solution, resulting in a 5 wt. % slurry. This suspension was subjected to ultrasonication (60 W) for 5 minutes to

ensure complete dispersion. After stabilization, the pH was checked and adjusted if necessary, followed by the addition of 5 mL of PAA solution. The mixture was then stirred using a magnetic stirrer and allowed to equilibrate for 2 hours. In experiments where the solid content was intentionally varied, the same protocol was followed with adjusted alumina-to-solution ratios. All adsorption experiments were performed in 20 cm^3 glass scintillation vials. Adsorption density (Γ) was calculated using the following equation (1):

$$\Gamma = \frac{(C_i - C_r) \times V_{sup}}{m_s \times s.a_s} \qquad [mg\ m^{-2}] \qquad (1)$$

- C_i is the initial polymer concentration (ppm of carbon)
- C_r is the residual (equilibrium) polymer concentration (ppm of carbon)
- V_{sup} is the volume of the supernatant (cm^3)
- m_s is the mass of solid (mg)
- $s.a_s$ is the specific surface area of the solid ($m^2\ g^{-1}$)

In the calculation of adsorption density, we used the carbon concentration in ppm (as indicated in the equation) or the total PAA concentration after applying a conversion factor of 2.04. This conversion factor is used to convert carbon ppm into PAA ppm, as PAA contains approximately 49 % carbon.

POLYMER CONCENTRATION MEASUREMENTS AND ADSORPTION PROCEDURE

Polymer concentrations were determined using a Dohlmann DC-90 Total Organic Carbon (TOC) analyzer, equipped with catalytic combustion at 900°C (Co_3O_4 catalyst) and infrared (IR) detection. After polymer addition, samples were stirred for 2 hours (based on preliminary kinetic studies confirming equilibrium), then centrifuged at 3,000 rpm for 30 minutes. The supernatant was collected for analysis, and adsorption values were normalized to the specific surface area (determined by BET analysis) to calculate surface coverage. Adsorption density was determined using the solution depletion method, as the difference between initial and residual PAA concentrations. This procedure was applied consistently for kinetic studies, where the variable was the mixing duration.

RESULTS AND DISCUSSION

Mineralogical Analysis by X-Ray Diffraction

The X-ray diffraction (XRD) patterns obtained for both AKP-50 and Linde alumina samples revealed the presence of a single crystalline phase, corresponding to α–Al_2O_3. According to the manufacturer, Linde alumina may contain up to 10 % γ–Al_2O_3. While the experimental data do not definitively confirm the presence of this secondary phase, the results suggest that, if present, the content of γ–Al_2O_3 does not exceed 3–4%. Representative diffraction patterns for both alumina samples are provided in Table 3 and in Supplementary Figures S1 and S2.

Mineral Characterization

SCANNING ELECTRON MICROSCOPY (SEM) AND ENERGY-DISPERSIVE X-RAY SPECTROMETRY (EDS)

Microscopic examination of particle morphology provides valuable insights into surface texture, degree of agglomeration, and porosity, all of which can significantly influence adsorption density behavior.[25] Scanning electron microscopy (SEM) was employed to assess the structural characteristics of the alumina powders after dispersion by ultrasonication. SEM images of the Linde A sample, recorded at lower magnification, revealed compact agglomerates composed of numerous smaller primary

Table 3. X -Ray Diffraction data for α–Al_2O_3.

d, Å	2Θ	I/I_o	hkl	*d*, Å	2Θ	I/I_o	Hkl
3.479	25.58	75	012	1.374	68.19	50	030
2.552	35.13	90	104	1.239	76.88	15	1010
2.379	37.78	40	110	1.190	80.69	7	220
2.085	43.36	100	113	1.147	84.37	5	223
1.740	52.55	45	024	1.126	86.37	5	312
1.601	57.52	80	116	1.099	89.01	7	0210
1.514	61.16	5	122	1.078	91.20	7	134
1.510	61.34	7	018	1.043	95.25	13	226
1.404	66.54	30	124	-	-	-	-

crystallites. These agglomerates appeared as "hard" clusters, indicating strong interparticle interactions. [25,26] At higher magnification, a pronounced porous structure was observed within the agglomerates, suggesting substantial internal surface area available for adsorption (Figure 1). In contrast, the SEM analysis of the AKP-50 alumina sample displayed well-separated, discrete particles that were nearly monodisperse in size and shape. The surfaces appeared smooth and compact, with no visible porosity or internal voids, consistent with the non-porous nature of this alumina (Figure 2). Energy-dispersive X-ray spectrometry (EDS) was performed in conjunction with SEM to confirm elemental composition. Both samples showed spectra characteristic of high-purity alumina, with no detectable foreign elements or impurities. These microstructural differences between the two alumina types, porous agglomerates in Linde A versus discrete, non-porous particles in AKP-50 are expected to play a key role in determining polymer adsorption behavior.

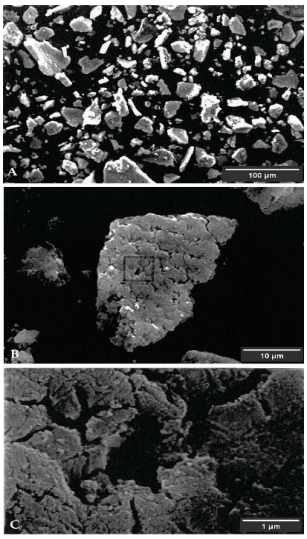

Figure 1. SEM micrographs of Linde A alumina: a) magnification: 250×; b) magnification: 2000×; c) magnification: 20000×.

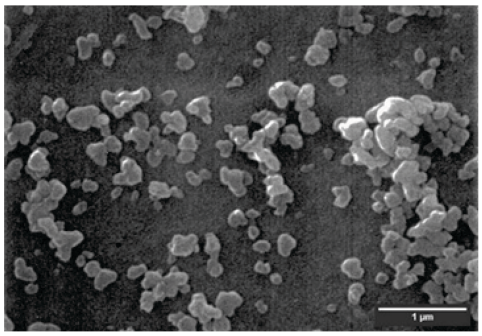

Figure 2. SEM micrographs of AKP-50 alumina (magnification: 20000×).

PARTICLE SIZE DISTRIBUTION

The particle size distribution of the two alumina samples was determined using different methods, based on the morphological characteristics observed via electron microscopy. For Linde A alumina, measurements obtained using the Microtrac forward light scattering system yielded a mean particle diameter of 19.9 µm. The corresponding particle size distribution is presented in Figure S3. This result deviates significantly from the manufacturer's reported value of 0.3 µm and aligns more closely with the SEM observations, which indicated the presence of larger agglomerates composed of smaller primary crystallites. The discrepancy is likely due to the presence of strongly bound agglomerates that are not completely disrupted during sample preparation. In the case of AKP-50 alumina, particle size measurements were performed using the Brookhaven Multi-Angle Light Scattering System. Given the nearly spherical and non-agglomerated morphology of this sample, as revealed by SEM, the obtained results are considered reliable. The calculated mean particle diameter was 267 nm, and the particle size distribution was narrow and symmetric, as shown in Table 4 and Figure S4. These findings are in good agreement with the manufacturer's specifications. Overall, the measured particle size distributions corroborate the morphological differences between the two alumina samples and are consistent with their respective synthesis routes and physical properties.

ZETA POTENTIAL

The zeta potential of alumina samples was measured in 0.03 mol dm^{-3} NaCl solution as background electrolyte, across a range of pH values. The results are presented in Figures S5 and S6 for Linde A and AKP-50, respectively. The use of a constant ionic strength was intended to eliminate variations in the electrical double layer thickness with changing pH [23]. The isoelectric point (IEP), defined as the pH at which the net surface charge of particles is zero, was estimated to be approximately pH 8.9 for AKP-50 alumina, and around pH 8.4 for Linde A alumina. These values are consistent with previously reported IEPs for high-purity α-Al_2O_3.

Table 4. Manufacturers data on AKP-50 alumina.

Diameter, nm	Particle number by intensity	Cumul., %	Diameter, nm	Particle number by intensity	Cumul., %
157	0	0	288	71	87
171	0	0	314	36	99
187	0	0	342	4	100
204	0	0	373	0	100
222	33	11	407	0	100
242	69	33	444	0	100
264	100	65	484	0	100

SPECIFIC SURFACE AREA BY NITROGEN ADSORPTION (BET METHOD)

The specific surface area of both alumina samples was determined using the multipoint Brunauer–Emmett–Teller (BET) method. Nitrogen adsorption measurements were carried out at 77 K, and five-point BET plots were constructed. The obtained isotherms and surface area data are shown in Figures S7 and S8. The calculated specific surface areas were found to be in agreement with values previously reported in the literature[24] and/or those provided by the respective manufacturers, confirming the reproducibility and reliability of the BET analysis.

PARTICLE POROSITY

The porosity of the alumina particles was assessed based on a combination of scanning electron microscopy and surface area data. For Linde A alumina, the significant discrepancy between the observed particle size and the measured specific surface area suggests the presence of substantial internal porosity. To further investigate this, two complementary methods were employed: nitrogen adsorption and mercury intrusion porosimetry. The hysteresis observed in the nitrogen adsorption/desorption isotherm provides a qualitative indication of total pore volume. A detailed isotherm, obtained by stepwise nitrogen adsorption and desorption at 77 K (50 points total), is presented in Figure 3. The average pore diameter calculated from these data was 274 Å.

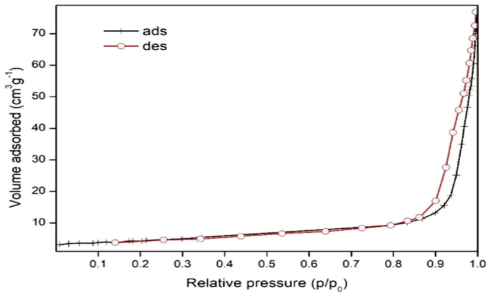

Figure 3. Adsorption/desorption isotherm of nitrogen on Linde A alumina at 77 K.

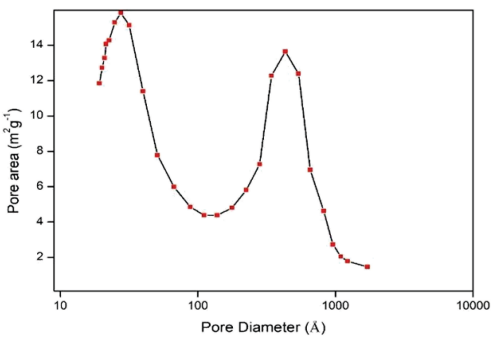

Figure 4. Desorption pore area plot for Linde A alumina.

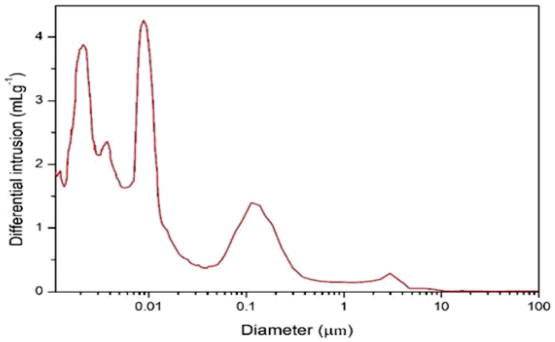

Figure 5. Pore distribution of Linde A alumina measured by mercury intrusion porosimetry.

Additionally, the desorption pore size distribution plot (Figure 4) revealed two prominent peaks at approximately 27 Å and 440 Å, indicating the presence of both mesopores and macropores within the Linde A agglomerates. The total porosity of Linde A alumina was measured as 82.85 % and the average pore diameter determined using Mercury intrusion porosimetry (25) is 0.21 μm. The inconsistency of pore diameter data obtained using the two different methods can be explained by comparison of Fig. 4 and 5. Summarizing the result obtained by porosity measurements of Linde A alumina it is evident that: (a) most (82.85 %) of the particle surface is in the pore interior, and (b) the distribution of pore sizes is not uniform. There are distinctive maxima at the pore diameters of 27, 55, 200, 2 000, and 40 000 Å.

EFFECT OF POLYMER MOLECULAR WEIGHT

It is well established in the literature that polymer adsorption density generally increases with increasing molecular weight, primarily due to the formation of thicker adsorbed layers on the substrate surface[12,26–28]. To investigate this effect systematically, adsorption experiments were conducted using polyacrylic acid (PAA) samples with molecular weights of 5000, 150000, and 800000 g mol^{-1}. Two alumina types were employed as adsorbents: porous Linde A and non-porous AKP-50.

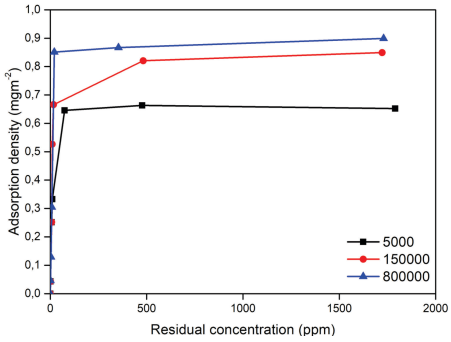

Figure 6. The adsorption density of PAA (M_w 5000, 150000, 800000) on AKP-50 alumina (pH 4, 0.03 mol dm^{-3} NaCl).

The results obtained at pH 4 are presented in Figures 6 and 7 and provide insight into the relationship between polymer molecular weight and adsorption behavior on substrates with distinct surface morphologies.

The obtained results stand in contrast to those commonly reported in the literature, where adsorption density typically increases with polymer molecular weight. Interestingly, in this study, the opposite trend was observed (Figure 7). A plot of maximum adsorption density as a function of polymer molecular weight is presented in Figure 8. The comparison of polymer molecular size with alumina pore structure suggests that lower molecular weight PAA exhibits higher adsorption density due to its greater ability to access internal pore surfaces. In contrast, larger polymer chains are likely excluded from narrow pores, leading to reduced adsorption density. This interpretation is further supported by results obtained at three different pH values (4, 7, and 10), as shown in Figure 9. The maximum adsorption density was found to decrease with increasing pH, which can be attributed to the reduced electrostatic attraction between the negatively charged polymer chains and the increasingly neutral or negatively charged alumina surface. At pH 10, adsorption plateaus for all molecular weights were nearly identical, indicating that under these conditions, extended polymer chains can penetrate the pore structure regardless of their length, rendering adsorption largely independent of molecular weight.

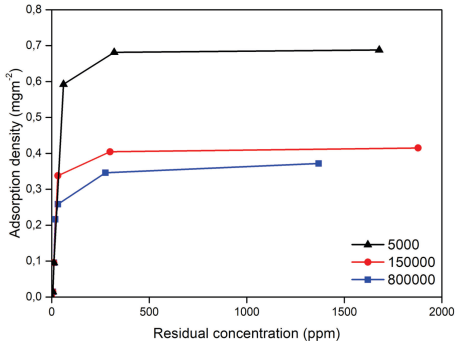

Figure 7. The adsorption density of PAA (Mw 5000, 150000, 800000) on Linde A alumina (pH 4, 0.03 mol dm^{-3} NaCl).

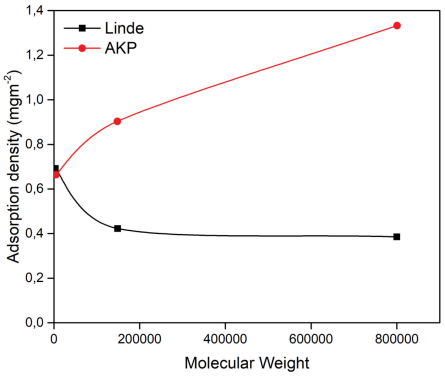

Figure 8. The adsorption density plateau as a function of PAA molecular weight.

EFFECT OF POLYMER MOLECULAR WEIGHT ON ADSORPTION BEHAVIOR

he results obtained in this study are in contrast with commonly reported literature data, which generally show that adsorption density increases with increasing polymer molecular weight. Surprisingly, the opposite trend was observed in the case of porous Linde A alumina (Figure 7). A plot of the maximum adsorption density as a function of polymer molecular weight is shown in Figure 8. The data clearly indicate higher adsorption for lower molecular weight polyacrylic acid (PAA), suggesting that the smaller polymer chains are more capable of penetrating the internal pore structure of the porous alumina. This behavior can be attributed to selective pore accessibility, where only smaller PAA molecules are able to diffuse into narrow pores, while larger, coiled chains are sterically excluded. These findings are consistent with pore structure data discussed previously and further supported by adsorption experiments conducted at three different pH values (4, 7, and 10), as shown in Figure 9. As pH increases, the maximum adsorption density decreases, which can be explained by the reduction in attractive electrostatic interactions between the negatively charged polymer and the increasingly neutral or negatively charged alumina

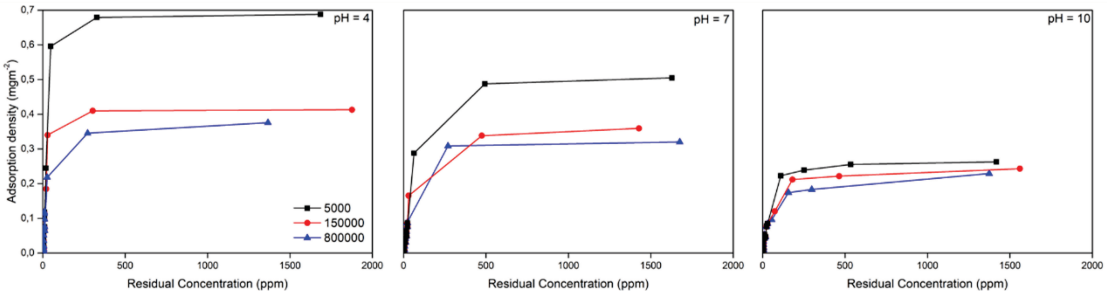

Figure 9. The effect of pH on the PAA adsorption density on Linde A alumina (0.03 mol dm^{-3} NaCl).

surface. Notably, at pH 10, adsorption plateaus for PAA of all molecular weights converge to nearly identical values. This suggests that, at high pH, polymer chains adopt a stretched conformation due to increased ionization, enabling even high molecular weight polymers to access the internal pore surfaces. As a result, adsorption becomes independent of chain length. In Figures 7, 8, and 9, the x-axes represent the initial concentration of PAA in solution, expressed in parts per million (ppm) of carbon (mg C/L), reflecting the use of a Total Organic Carbon (TOC) analyzer for quantification. Given that PAA contains approximately 49 % carbon by weight, the total polymer concentration (mg L^{-1}) can be estimated by applying a conversion factor of 2.04. For instance, a solution with 100 ppm of carbon corresponds to approximately 204 ppm of total PAA. The y-axes show the amount of polymer adsorbed onto the alumina surface (mg g^{-1}), as determined by the solution depletion method. Using the specific surface area of Linde A alumina (15 m^2 g^{-1}, based on BET analysis), surface coverages were estimated. At pH 4, maximum adsorption densities ranged from 3.5 to 5.0 mg g^{-1}, depending on polymer molecular weight, corresponding to surface coverages of approximately 0.23 to 0.33 mg m^{-2}. Considering the estimated footprint of coiled PAA molecules which increases with molecular weight these values suggest the formation of partial to near-complete monolayers. The observed decrease in adsorption density with increasing molecular weight (on Linde A) is consistent with restricted accessibility of larger polymer coils to internal pore surfaces. Conversely, at elevated pH where the polymers are more extended, the influence of molecular size on pore accessibility diminishes, leading to adsorption behavior that is largely independent of polymer size. This analysis also clarifies the relationship between TOC-derived carbon concentrations and total polymer content, providing a quantitative basis for interpreting the observed adsorption trends.

INFLUENCE OF POLYACRYLIC ACID DISSOCIATION ON ADSORPTION BEHAVIOR

The adsorption behavior of polyacrylic acid (PAA) on alumina surfaces is strongly influenced by its degree of dissociation, which is pH-dependent. As a weak polyelectrolyte with a dissociation constant (p*K*a) typically in the range of 4.5–5.5, PAA exhibits significant changes in charge density and molecular conformation with varying pH. At low pH values (e.g., pH 4), the majority of carboxylic acid groups remain protonated, resulting in a neutral or only slightly negatively charged polymer. Under these conditions, reduced intramolecular electrostatic repulsion causes PAA chains to adopt a compact, coiled conformation. This conformation facilitates the entry of lower molecular weight PAA chains into the narrow pores of porous alumina (Linde A), which is consistent with the observed inverse relationship between molecular weight and adsorption density (Figure 7). These findings support the conclusion that steric accessibility, rather than electrostatic interaction, dominates the adsorption process under acidic conditions.

In contrast, at high pH values (e.g., pH 10), PAA becomes highly ionized. The resulting increase in electrostatic repulsion along the polymer chain leads to an extended, rod-like conformation. Simultaneously, the alumina surface also becomes more negatively charged at higher pH, as evidenced by zeta potential measurements (Figures S5 and S6), further increasing electrostatic repulsion between the polymer and the substrate. Consequently, the overall adsorption density decreases with increasing pH, as shown in Figure 9. Notably, at pH 10, adsorption plateau values converge for all polymer molecular weights. This suggests that molecular conformation, rather than size, becomes the dominant factor governing adsorption behavior. When PAA chains are fully stretched, even higher molecular weight species are able to access surface regions previously limited by steric hindrance under coiled conformations. These trends are in agreement with literature data on weak polyelectrolytes [26–28] and highlight the importance of considering the degree of ionization when interpreting adsorption behavior. The observed pH-dependent variation in adsorption reflects the combined influence of three interrelated factors: (i) polymer ionization, (ii) molecular conformation, and (iii) surface charge of alumina. Each of these factors changes systematically with pH and contributes to the complex interplay that determines the extent of polymer adsorption density [12,26–28]

CORRELATION BETWEEN PORE SIZE AND POLYMER MOLECULAR SIZE

Based on the combined results of alumina morphological characterization and adsorption experiments under various conditions, a conceptual adsorption model is proposed, as illustrated schematically in Figure 10. The model is built on two key observations: (a) At low pH, where PAA chains adopt a coiled conformation, adsorption on porous Linde A alumina is inversely proportional to the polymer molecular weight. This is attributed to the preferential access of smaller coils into the pore network. (b) At high pH, where PAA chains are highly ionized and adopt a stretched

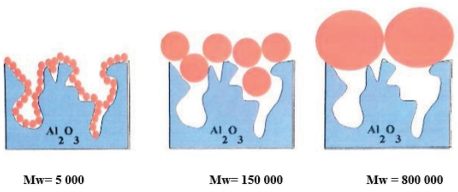

Figure 10. Schematic model of polymer adsorption on porous alumina at low pH (4).

conformation, adsorption becomes independent of molecular weight, as even larger chains are able to interact with the pore surfaces due to reduced steric hindrance. A comparison of alumina pore sizes determined by porosity measurements with the calculated molecular dimensions of PAA at pH 4 is presented in Table 5. This correlation further supports the proposed mechanism of size-selective adsorption and highlights the critical role of polymer conformation and substrate porosity in determining adsorption behavior [12,22]

The polymer of the lowest molecular weight can enter all but smallest pores of the alumina substrate. The larger molecules (higher molecular weight polymers) can penetrate only into pores with diameter bigger than their respective molecular sizes: for polymer of M_w 150000 pores with diameter 27, 55 and 91 Å are inaccessible while polymer of M_w 800000 can enter only pores larger than 200 Å.

The results of this study revealed an inverse relationship between the molecular weight of polyacrylic acid (PAA) and its adsorption density on porous alumina (Linde A) at pH 4. This finding stands in contrast to numerous reports in the literature, which frequently observe an increase in adsorption with increasing polymer molecular weight particularly on non-porous substrates. Santhiya et al. (1998)[29] investigated PAA adsorption on non-porous α-Al_2O_3 and reported a positive correlation between molecular weight and adsorption density. This was attributed to enhanced segmental interactions, the presence of multiple anchoring points, and the ability of longer chains to form extended loops and tails at the surface. Momota et al. (2002)[30] examined the thermodynamics of PAA adsorption on alumina and found that the enthalpy of adsorption transitioned from endothermic to exothermic as molecular weight decreased at pH 8. At pH 10, adsorption was endothermic for all molecular weights.

These observations reinforce the role of polymer conformation and ionization state in determining adsorption energetics. Chen (2007)[31] reported significantly higher PAA adsorption on α-Al_2O_3 at low pH (3.6) compared to high pH (11), confirming the strong influence of polymer ionization and surface charge.

Table 5. Polymer molecular size and pore sizes of Linde A alumina.

Polymer M_w	Polymer diameter, Å	Pore diameter, Å
5000	30	27 55 91
150000	163	200
800000	375	2000 40000

While molecular weight was not the focus of that study, the observed pH sensitivity is consistent with our findings. Jeon and Hong (2003)[32] further demonstrated that both pH and molecular weight significantly affect PAA adsorption on alumina, with higher adsorption density at lower pH attributed to favorable electrostatic and hydrogen bonding interactions. Wiśniewska et al. (2013) [33] studied PAA adsorption on silica–alumina mixed oxides and observed a decrease in adsorption density with increasing pH, due to the reduced availability of protonated carboxyl groups and increased electrostatic repulsion from the negatively charged surface. Wiśniewska et al. (2016)[34] showed that lower molecular weight PAA adsorbed more effectively onto porous activated carbon at low pH, which they attributed to improved accessibility of internal pore surfaces, an effect directly relevant to our system. Collectively, these literature reports support the view that polymer conformation and pore accessibility are dominant factors controlling adsorption, particularly under acidic conditions.

Our findings align with this framework and extend it to show that, for porous substrates like Linde A alumina, the steric exclusion of larger, coiled PAA chains leads to a reversal of the classical molecular weight–adsorption relationship. At higher pH values, where PAA chains become fully ionized and adopt stretched conformations, adsorption density becomes largely independent of molecular weight. This confirms that under such conditions, the extended conformation enables even high-molecular-weight polymers to access internal pore surfaces, thereby diminishing the influence of molecular size.

CONCLUSION

This study explored the adsorption behavior of polyacrylic acid (PAA) with varying molecular weights on two types of alumina substrates porous (Linde A) and non-porous (AKP-50) over a pH range of 4 to 10. The findings reveal that adsorption density is governed by a complex interplay between polymer molecular weight, pH-dependent ionization, and substrate morphology. In contrast to widely reported trends observed on smooth or non-porous surfaces, our results show that on porous alumina, lower molecular weight PAA exhibits higher adsorption density, particularly at low pH where the polymer adopts a coiled conformation. This behavior is attributed to improved steric accessibility of smaller polymer chains into internal pore structures. At elevated pH values, PAA becomes highly ionized and extended, leading to reduced adsorption density across all molecular weights and converging adsorption densities. These observations underscore the importance of matching polymer coil size with substrate

pore architecture when designing efficient dispersants or surface modifiers. Electrokinetic measurements and adsorption data collectively demonstrate that pH-dependent polymer ionization, combined with steric exclusion and electrostatic interactions, critically influence adsorption mechanisms. Our comparative analysis with literature further contextualizes these results, offering a consistent framework for understanding deviations from classical adsorption models. Importantly, this work highlights the necessity of moving beyond idealized surfaces in adsorption studies and accounting for morphological parameters such as porosity when evaluating polymer–surface interactions. Future studies should extend this approach to other polyelectrolytes and more complex or composite materials, in order to develop a deeper, more realistic understanding of polymer adsorption in practical and industrially relevant systems.

Supplementary Information. Supporting information to the paper is attached to the electronic version of the article at: https://doi.org/10.5562/cca4170.

PDF files with attached documents are best viewed with Adobe Acrobat Reader which is free and can be downloaded from Adobe's web site.

REFERENCES

[1] C. Monteux, *C. R. Phys.* **2014**, *15*, 775–785. https://doi.org/10.1016/j.crhy.2014.10.002https://doi.org/10.1016/j.crhy.2014.10.002

[2] Polymer Science and Engineering: The Shifting Research Frontiers. National Research Council. **1994**, Washington, DC: The National Academies Press

[3] S. Farrokhpay, *Adv. Col. Inter. Sci.* **2009**, *15*, 24–32. https://doi.org/10.1016/j.cis.2009.07.004

[4] B. Zhu, T. Gu, *Adv. Coll. Inter. Sci.* **1991**, *37*, 1–32. https://doi.org/10.1016/0001-8686(91)80037-k

[5] R. Atkin, V. Craig, E. Wanless, S. Biggs, *Adv. Col. Inter. Sci.* **2003**, *103*, 219–304. https://doi.org/10.1016/S0001-8686(03)00002-2

[6] S. Oppo, V. Fiorentini, M. Scheffler, *Phys. Rev. Lett.* **1991**, *71*, 2437–2440. https://doi.org/10.1103/PhysRevLett.71.2437

[7] K. Urano, M. Saito, C. Murata, *Chemosphere* **1984**, *13*, 293–300. https://doi.org/10.1016/0045-6535(84)90136-X

[8] B. Theng, *Polymer Behavior at Clay and Solid Surfaces* **1979**, *n/a*, 37–61. https://doi.org/10.1016/S0166-2481(08)70113-2

[9] S. Bauyrzhan. Adsorption/Retention of Polymer Solution in Porous Media. Mechanics [physics]. Université de Bordeaux, **2021**. Doctoral Thesis.

[10] U. Raviv, J. Klein, *Poly. Sci.* **2012**, *2*, 607–682. https://doi.org/10.1021/jp0041860

[11] M. Wiśniewska, G. Fijałkowska, K. Szewczuk-Karpisz, *Chemosphere* **2018**, *211*, 524–534. https://doi.org/10.1016/j.chemosphere.2018.07.198

[12] W. Xu, K. Mihhels, N. Kotov, S. Lepikko, R. Ras, C. Johnson, E. Kontturi, *J. Colloid Interface Sci.* **2022**, *605*, 441–450. https://doi.org/10.1016/j.jcis.2021.07.062

[13] J. Willott, T. Murdoch, F. Leermakers, W. de Vos, *Macromolecules* **2018**, *3*, 1198–1206. https://doi.org/10.1021/acs.macromol.7b02244

[14] M. Reches, P. Snyder, G. Whitesides, *PNAS* **2009**, *42*, 17644–17649. https://doi.org/10.1073/pnas.0905533106

[15] H. Vutukuri, *Colloids* **2012**, *70*, 1–6. https://doi.org/10.1002/anie.201202592

[16] S. Cohen, *Adv. Col. Inter. Sci.* **1986**, *24*, 143–239.

[17] Y. Lin, A. Frischnecht, K. Winey, *J. Chem. Phys.* **2021**, *155*, 1–76. https://doi.org/10.1063/5.0052121

[18] T. Tadros, *Polymeric Surfactants* **2017**, *n/a*, 37–64. https://doi.org/10.1515/9783110487282-005

[19] K. Onita, M. Onishi, T. Omura, T. Wakiya, T. Suziki, H. Minami, *Langmuir* **2022**, *38*, 7341–7345. https://doi.org/10.1021/acs.langmuir.2c00946

[20] J. Ugelstad, H. Mfutakamba, P. Mork, *J. Pol. Sci.* **2007**, *72*, 226–240.

[21] A. Papadopoulou, J. Gillisen, M. Tiwari, S. Balabani, *Materials* **2020**, *13*, 1–17. https://doi.org/10.3390/ma13204628

[22] M. Wedd, *Enc. Anal. Sci.* **2005**, *161*, 18–29. https://doi.org/10.1016/B0-12-369397-7/00439-8

[23] S. Celik, *Inter. Sci. Techn.* **2004**, *1*, 57–89. https://doi.org/10.1016/S1573-4285(04)80037-1

[24] P. Temmerman, *J. Nanobio.* **2012**, *10*, 1–11. https://doi.org/10.1186/1477-3155-10-24

[25] S. Mikmekova, T. Aoyama, *Ultramicroscopy* **2024**, *220*, 113965–113965. https://doi.org/10.1016/j.ultramic.2024.113965

[26] Y. Nikas, D. Blankschtein, *Langmuir* **1994**, *10*, 3512–3528. https://doi.org/10.1021/la00022a026

[27] Y. Shin, E. Roberts, M. Santore, *J. Coll. Interf. Sci.* **2002**, *247*, 220–230. https://doi.org/10.1006/jcis.2001.8100

[28] M. Wiśniewska, K. Terpilowski, S. Chibowski, T. Urban, *Pow. Tech.* **2013**, *233*, 157–163. https://doi.org/10.1016/j.powtec.2012.08.037

[29] D. Santhiya, G. Nandini, K. Natarajan, S. Malghan, *Colloids Surf. B: Biointerfaces* **1998**, *133*, n/a–n/a. https://doi.org/10.1016/S0927-7757(97)00132-5

[30] M. Momota, S. Tanaka, N. Uchida, K. Uematsu, *Key Eng. Mater.* **2001**, *95*, 206–213. https://doi.org/10.4028/www.scientific.net/KEM.206-213.95

[31] H. Chen, *J. Am. Ceram. Soc.* **2007**, *90*, 1709–1709. https://doi.org/10.1111/j.1551-2916.2007.01644.x

[32] S. Jeon, W. Hong, *Korean J. Chem. Eng.* **2003**, *20*, 916–921. https://doi.org/10.1007/BF02697299

[33] M. Wiśniewska, T. Urban, E. Grządka, V. Zarko, V. Gun'ko, *Colloid Polym. Sci.* **2014**, *292*, 699–705. https://doi.org/10.1007/s00396-013-3103-x

[34] M. Wiśniewska, A. Nosal-Wiercińska, I. Ostolska, D. Sternik, P. Nowicki, R. Pietrzak, A. Bazan-Wozniak, O. Goncharuk, *Nanoscale Res. Lett.* **2017**, *12*, 1–9. https://doi.org/10.1186/s11671-016-1772-3